Electronic correlations and pressure-induced metallicity in LaMnPO_{1−x}F_{x} revealed via infrared spectroscopy

K. W. Post, Alexander F. Goncharov, Z. P. Yin, J. W. Simonson, Jing Guo, Liling Sun, S. Zellman, M. D. Goldflam, H. T. Stinson, B. C. Chapler, D. E. McNally, Zhongxian Zhao, G. Kotliar, M. C. Aronson, and D. N. Basov

Phys. Rev. B **94**, 045115 — Published 14 July 2016

DOI: 10.1103/PhysRevB.94.045115

On electronic correlations and pressure induced metallicity in $LaMnPO_{1-x}F_x$ revealed via infrared spectroscopy

K.W. Post,[1,*], Alexander F. Goncharov,[2] Z.P. Yin,[3] J.W. Simonson,[4] Jing Guo,[5] Liling Sun,[5] S. Zellman,[4] M.D. Goldflam,[1] H.T. Stinson,[1], B.C. Chapler,[1] D.E. McNally,[4], Zhongxian Zhao,[5], G. Kotliar,[3] M.C. Aronson,[4,6,7] and D.N. Basov[1,8]

[1] *Physics Department, University of California-San Diego, La Jolla, California 92093, USA*

[2] *Geophysical Laboratory, Carnegie Institution of Washington, 5251 Broad Branch Road NW, Washington, DC 20015, USA*

[3] *Department of Physics and Astronomy, Rutgers University, Piscataway, NJ 08854, USA*

[4] *Department of Physics and Astronomy, Stony Brook University, Stony Brook, NY 11794*

[5] *Institute of Physics and Beijing National Laboratory for Condensed Matter Physics, Chinese Academy of Sciences, Beijing 100190*

[6] *Condensed Matter Physics and Materials Science Department, Brookhaven National Laboratory, Upton, NY 11937 USA*

[7] *Department of Physics, Texas A&M University, College Station, TX 77843, USA*

[8] *Department of Physics, Columbia University, New York, New York 10027, USA*

We spectroscopically investigated the energy gap of the correlated antiferromagnetic insulator $LaMnPO_{1-x}F_x$ (x=0.0 and 0.04) as a function of temperature and pressure, separately, in conjunction with many body electronic structure calculations. These results show that the electronic structure in all measured regimes is well described by a model that includes both Mott-Hubbard interactions and Hund's rule coupling. Moreover, we find that by appying external pressure, thereby reducing the effective Mott-Hubbard interaction and Hund's coupling, the energy gap in $LaMnPO_{1-x}F_x$ can be fully closed, yielding a metallic state.

I. INTRODUCTION

Progress in the physics of correlated electron systems is often initiated by the discovery of new materials that feature complex interplay between charge, spin and orbital degrees of freedom. One such class of materials are the recently synthesized Mn-pnictides. Initial reports on the insulating materials $BaMn_2As_2$, $CaMn_2Sb_2$, LaMnPO, LaMnAsO and LiMnAs suggests that these compounds possess rich phase diagrams, highlighting the importance of electronic correlations[1–10]. Typically, these systems form as antiferromagnetically (AF) ordered insulators with many bands residing in the vicinity of the Fermi energy. The electronic correlations of such multiband systems are often not well described solely with the Hubbard interaction (U), which only considers Coulomb repulsion of interacting carriers. Rather, the interaction of the carriers through the spin channel, via Hund's coupling (J_H) may also be necessary[11]. In the case of LaMnPO, recent work has suggested that it is a Mott-Hund's insulator, meaning both U and J_H act in concert to reproduce the observed insulating ground state[5,12]. Accordingly, this new system warrants detailed examination, as many exotic phenomena, such as quantum criticality, phase separation, and high temperature superconductivity often appear when correlated antiferromagnetic systems are metallized.

In this work, we have spectroscopically probed the energy gap (E_{Gap}) of the AF insulator LaMnPO in the high pressure (HP) and high temperature (HT) regimes. The power of infrared spectroscopy, in the context of unresolved issues related to LaMnPO, is that it is the only experimental technique that can directly probe the electronic band structure at both high pressures and elevated temperatures. These measurements were also carried out on $LaMnPO_{0.96}F_{0.04}$, as doping in other correlated AF systems has frequently led to exotic phenomena[13]. Our results reveal that E_{Gap} in both undoped and doped LaMnPO, is reduced from 1.0 eV in the AF state, to 0.85 eV in the para-magnetic (PM) state at 725K, a reduction of only 15%. In contrast, by applying pressure, E_{Gap} in $LaMnPO_{1-x}F_x$ (x=0.0, 0.04) is systematically reduced, yielding a full gap collapse above 20 GPa. The combined high pressure and high temperature measurements show that the band collapse is not caused by the elimination of AF order or the pressure induced structural transition near 16.2 GPa. The optical data, combined with DFT+DMFT calculations establish a realistic description of the LaMnPO ground state, and provide quantitative estimates of the U and J_H that govern the electronic structure. Additionally, we can unambiguously show that the emergent charge carriers at high pressures arise from a collapsed band within the bulk, thereby excluding alternative interpretations of the metallic state[6,14].

II. EXPERIMENTAL TECHNIQUES AND DISCUSSION

A. Sample Growth.

Single crystals of $LaMnPO_{1-x}F_x$ were grown from a NaCl-KCl eutectic flux. The crystals formed as thin plates of dark luster with typical dimensions of 1mm × 1mm × 5μm. The sample thickness of 5μm was confirmed both by modelling the raw transmittance spec-

tra while matching the periodicity of the interference fringes and by inspection. Doping with fluorine was accomplished by introducing MnF_2 powder to the samples prior to the crystal growth process. The F concentration of the synthesized crystals was determined via potentiometric measurements, as described previously[6], and the crystal structure was confirmed by single crystal x-ray diffraction.

B. High Temperature Measurements

Transmittance spectra of undoped and doped LaMnPO were measured from 0.01 to 1.5 eV, at temperatures ranging from 295K to 450K. The measurements of undoped LaMnPO, in the spectral range near E_{Gap} (0.8 eV $< \omega <$ 1.1 eV) were extended up to 725K using a custom elevated temperature sample stage. The raw transmittance data for undoped and doped LaMnPO, at 295K, are shown in Fig. 1a and 1b, respectively. The magnitude of E_{Gap} is extracted from the absorbance (αt), where α is the absorption coefficient of the material, and t is the sample thickness. Assuming incoherent transmittance, as appropriate in the case of limited experimental resolution or non-parallel crystal surfaces, absorbance is related to the absolute transmittance $T(\omega)$ and reflectance $R(\omega)$ via[15]:

$$T(\omega) = \frac{(1 - R(\omega))^2 e^{-\alpha t}}{1 - R(\omega)^2 e^{-2\alpha t}}. \quad (1)$$

Near the energy gap, where $R(\omega)$ is a nearly frequency independent value of R_0[16], the lineshape of αt is approximately given by $-\log(T(\omega))$. The $(1-R_0)^2$ correction to the $(\alpha t)^2$ spectra, which accounts for the reflectivity at the interface between the sample and the high pressure medium, is within the error bars of E_{Gap}, as discussed in sectionV. Likewise, since αt is large near the band gap, the denominator $1 - R(\omega)^2 e^{-2\alpha t} \approx 1$. In the case of a direct gap material, the x-axis intercept of a linear fit to $(\alpha t/\omega)^2$ yields E_{Gap}[16,17]. The $(\alpha t)^2$ spectra (colored lines), corresponding to the measured values of transmittance, are plotted in Fig. 1c and 1d, along with the linear fits to $(\alpha t/\omega)^2$ (dashed gray lines).

The values of E_{Gap} obtained from the absorption spectra are plotted as a function of temperature in Fig. 1e. The shadowed region in the inset of Fig. 1e highlights an area in the vicinity of the bulk Neél temperature (T_N) of 375K$\pm$5K. There is no abrupt change in E_{Gap} upon crossing the bulk AF to paramagnetic (PM) transition in either the undoped or doped samples. Additionally, E_{Gap} of the doped samples follows a trajectory very similar to the undoped sample, albeit at a slightly lower energy.

The resilience of E_{Gap} to temperature suggests that long-range AF correlations do not play a major role in defining the electronic structure of LaMnPO. However, prior work has demonstrated that short range AF correlations persist up to 700K[12]. We explored the effect of these remaining AF correlations on E_{Gap} by measuring the transmittance of undoped LaMnPO, at temperatures up to 725K. There is a slight discontinuity in the temperature dependence of E_{Gap} between 450K and 500K, which we attribute to changes in the experimental setup, necessary to accommodate temperatures above 450K. In this extended temperature range, E_{Gap} of undoped LaMnPO monotonically decreases with increasing temperature. Upon reaching the completely PM state at 725K[12], the energy gap is only 0.85 eV, which is 0.15 eV lower than E_{Gap} at 295K.

The value of E_{Gap} predicted from DFT+DMFT calculations in the AF (PM) state is indicated by the blue triangles at 300K (700K) with the corresponding band structure calculations shown in Fig. 1f (1g). These calculations predicted that the elimination of AF order reduces E_{Gap} by 0.12 eV, closely matching our experimentally measured values in the PM state. Therefore, while it is likely that the short-range AF correlations contribute to the 1.0 eV energy gap in $LaMnPO_{1-x}F_x$, they cannot produce it alone. Rather, the energy gap is stabilized primarily by the Hubbard U in concert with the Hund's J_H. This stands in stark contrast to theoretical work on the cuprates, where it has been suggested that the energy gap of the insulating parent compounds would not exist without the AF order[18].

C. High Pressure Measurements

To further explore the role of electron interactions in producing the optical gap, we examined the pressure dependence of the absorption edge in both the undoped and doped LaMnPO samples. In general, the application of pressure increases the electron kinetic energy, and may be expected to reduce the effect of electron correlations[19]. Of additional interest is the tetragonal to orthorhombic structural transition in LaMnPO near 16.2 GPa, and its affect on the electronic structure, which we are able to explore with these high pressure measurements[4].

The high pressure data were obtained using an FTIR spectrometer, coupled to a diamond anvil cell (DAC) in which cryogenically loaded nitrogen was used as the pressure medium[20]. The limited size of the DAC required sample dimensions that were less than $40\times40\times15$ μm^3. Due to limitations imposed by the low energy cut-off of the detector, and the diffraction limit related to the small sample size, energy gap values below 0.12 eV could not be measured. Furthermore, accurate measurement of transmittance was not possible in the region near 0.25 eV, due to absorption in the diamond anvil.

Transmittance spectra near E_{Gap} were obtained at a series of increasing pressures (P). The corresponding $(\alpha t)^2$ spectra are plotted in Fig. 2a and 2b, for $x = 0.0$ and $x = 0.04$, respectively, where the increase in $(\alpha t)^2$ indicates the onset of interband transitions. The absorption edge is systematically and rapidly suppressed with increasing P. The maximum P, at which a well

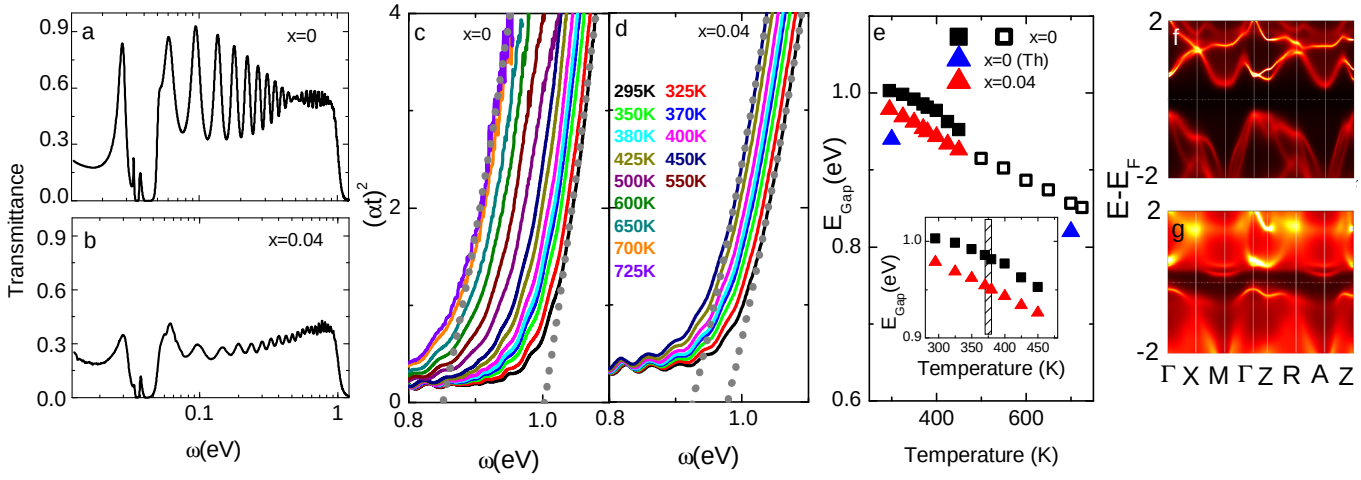

FIG. 1. Transmittance spectra of $LaMnPO_{1-x}F_x$ for $x = 0.0$ and $x = 0.04$ are plotted in panels (a) and (b), respectively. The corresponding absorption spectra $(\alpha t)^2$ are plotted in (c) for x=0 and (d) for x=0.04. The dashed gray lines plotted on top of the experimental (colored) lines show the linear fit to the $(\alpha t/\omega)^2$ form at the highest and lowest temperatures for each sample. The colored in (d) indicates the measurement temperature of the correspondingly colored spectra for both samples. The x-axis intercept of these linear fits were used to determine the value of the optical gap, E_{Gap}. The value of E_{Gap} extracted from the linear fit is plotted as a function of temperature in (e). We do not observe any anomalies in E_{Gap} upon crossing T_N (shadowed in the inset). The energy gap obtained from transmittance measurements at temperatures greater than 450 K are indicated by the open squares. Band structure calculations are shown for the AF (f) and PM (g) state, revealing a reduced direct energy gap at the Γ point in the PM state. The E_{Gap} values calculated for LaMnPO in the AF and PM states are indicated in (e) by the blue triangles at 300K and 700K, respectively.

defined absorption edge is still observable, defined as $P^*_{x=0}$ ($P^*_{x=0.04}$), is 18.8 GPa (15.1 GPa) for the undoped (doped) sample. These pressures are indicated in Fig. 2f, 2g and 2h. At P above P*, the well defined absorption edge is obscured by the appearance of intra-gap absorption features, which will be discussed later in the text. Accordingly, we only extracted a numerical value of E_{Gap} for $P \leq P^*$.

To determine E_{Gap} of the $LaMnPO_{1-x}F_x$ samples under high pressure, we utilized the same method employed for the high temperature data, with linear fits to $(\alpha t/\omega)^2$ indicated by the dashed gray lines in Fig. 2a (2b) for x=0.0 (x=0.04). The extracted values of E_{Gap} for both undoped and doped samples are plotted as a function of pressure in Fig. 2c. For $P < P^*$, the reduction of E_{Gap} obeys an approximately linear relationship with pressure. Assuming this trend continues for $P > P^*$, we performed a linear fit of the lower pressure E_{Gap} values to estimate the pressure at which the gap closes, *i.e.* E_{Gap}=0. These linear fits, indicated for the undoped (doped) sample by the black (red) dotted line in Fig. 2a, suggest that gap closure would occur at P=28 GPa (P=25 GPa).

For comparison, DFT+DMFT calculations were carried out for undoped LaMnPO at a series of pressures, with details of the calculations detailed in section IV. The smallest direct energy gap in the calculated band structure is plotted as the green circles in Fig. 2c. Below 16.2 GPa, the pressure dependence of the theoretical E_{Gap} is well captured by a linear fit, indicated by the green dotted line in Fig. 2c. Increasing the pressure to 16.2 GPa produces a more rapid decrease in E_{Gap}, which deviates from the linear trend found at P≤14 GPa, similar to behavior of the experimentally determined E_{Gap}. Full gap closure is theoretically anticipated to occur by 30 GPa[5], where the corresponding metallic band structure, calculated via DFT+DMFT, is shown in Fig. 3c. For direct comparison between the experimental data and theoretical results, the optical conductivity ($\sigma_1(\omega)$) spectra were extracted from the DFT+DMFT calculations. The $\sigma_1(\omega)$ spectra were then converted to $(\alpha t)^2$ (plotted in Fig. 2i) via the relationship[16]:

$$\alpha = \frac{4\pi\sigma_1}{n(\omega)c}, \tag{2}$$

where a Kramers-Krönig inversion of σ_1 was used to obtain $n(\omega)$, and $t = 5\mu m$. These spectra show a systematic suppression of the absorption edge, similar to the experimentally obtained absorbance spectra shown in Fig. 2a and 2b. Moreover, absorption peaks in the theoretical $(\alpha t)^2$ spectra appear above the tetragonal to orthorhombic phase transition at 16.2 GPa. These peaks are due to interband transitions at the M-point, which become allowed in the orthorhombic phase as can be seen in Fig. 3b, and qualitatively resemble the absorption features that are experimentally observed, and highlighted in Fig. 2d and 2e. Also, it is this structural transition

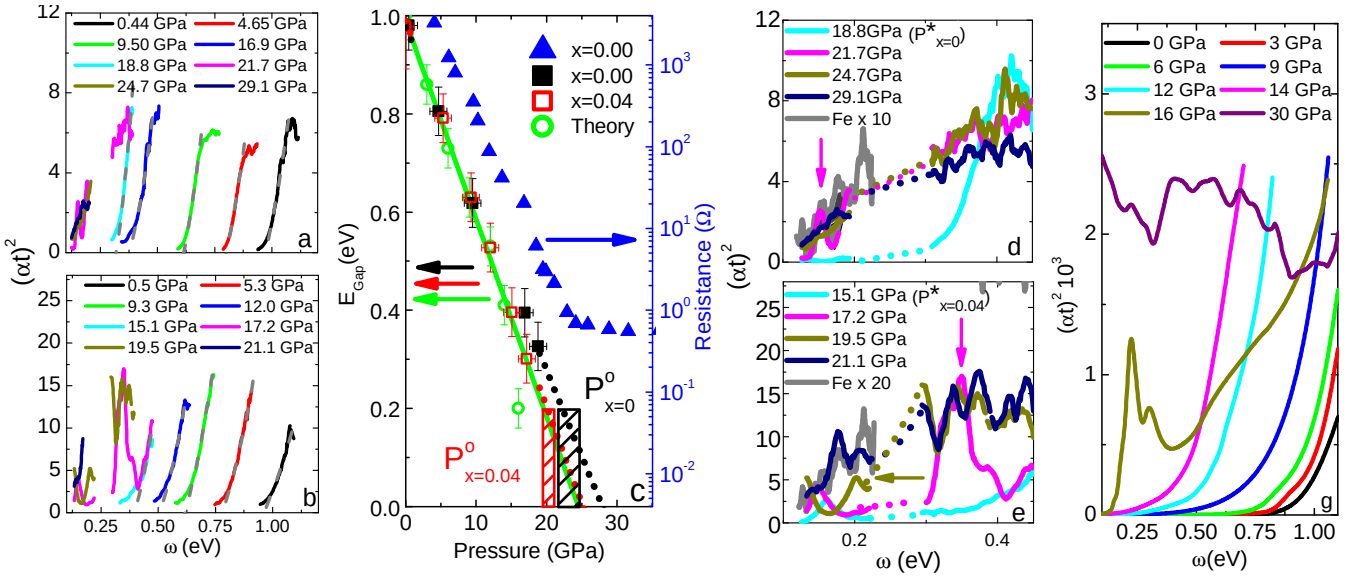

FIG. 2. In (a) and (b) we plot the $(\alpha t)^2$ spectra of $LaMnPO_{1-x}F_x$, for x=0.0 and x=0.04 respectively, at a series of increasing pressures. The dashed gray lines indicate the linear fits to $(\alpha t)^2/\omega^2$ which are used to determine the value of E_{Gap}. Above 18.8 GPa in (a), and above 15.1 GPa in (b) peaks appear in the $(\alpha t)^2$ spectra, which are detailed in (f) and (g). In (c) the value of E_{Gap} that we extracted for undoped (doped) LaMnPO are plotted as the black filled squares (red open squares). The black (red) lined rectangles indicate the pressure over which we metallicity emerges in the undoped (doped) sample. Complementary high pressure resistance data for the undoped sample (x=0.00) are plotted in blue, corresponding to the right axis, which was taken from[14]. The green, open circles, indicate the smallest direct energy gap determined from DFT+DMFT electronic structure calculations. The green dotted line shows the linear relationship between the theoretical E_{Gap} and pressure for P$\leq$ 14 GPa. The low ω region of the $(\alpha t)^2$ spectra, of both undoped and doped LaMnPO are highlighted in (f) and (g), where P^*_x is indicated in the legend. In the undoped $(\alpha t)^2$ spectra, where the applied pressure was 21.7 GPa, there appears to be a small peak at 0.15 eV, indicated by the pink arrow. Likewise, in the $(\alpha t)^2$ spectra of the doped sample, there is a pronounced peak at 0.35 eV when P=17.2 GPa (indicated by the pink arrow), and increasing the pressure to 19.5 GPa yields a small peak at 0.19 eV (yellow arrow). The Further application of pressure results in the suppression of these intra-gap features. For further comparison between theory and experiment, in (f) we have plotted the $(\alpha t)^2$ spectra, extracted from DFT+DMFT electronic structure calculations. The 16 GPa and 30 GPa $(\alpha t)^2$ spectra have been scaled by 0.05 and 0.02, respectively, so that they can be seen alongside the lower pressure spectra.

that produces the deviation from linearity in the theoretically predicted values of E_{Gap} at 16.2 GPa, described earlier in the text. Interestingly, the intra-gap absorption peaks that indicate the tetragonal to orthorhombic transition in the theoretical absorption spectra at 16.2 GPa, do not appear in our experimental data until pressures greater than 18.8 GPa. We attribute this to differences in the level of uniaxial pressure between the pressure medium used in the x-ray diffraction measurements, and our transmittance measurements. This latter fact, in conjunction with the error bars inherent in high pressure measurements, can account for the difference in the pressures at which the intra-gap peaks emerge.

As stated earlier in the text, the band edge at high pressures is obscured by the intra-gap absorption peaks, which make it difficult to precisely determine the pressure at which the gap collapses. One method to estimate the pressure where the energy gap is fully closed is to compare our measured absorption spectra, to that obtained for a known metallic sample. Accordingly, we measured the absorbance of an iron (Fe) flake in the same experimental setup used for the high pressure measurements. The absorbance spectra of Fe is plotted alongside the high pressure absorbance spectra of LaMnPO in Fig. 2d and 2e as the gray solid line. The Fe sample that we used was smaller than either the undoped or doped LaMnPO sample. Thus, it's absorption was notably smaller at low ω due to diffraction of light around the small sample. Regardless, the absorbance of Fe is plotted alongside that of undoped (doped) LaMnPO in Fig. 2d and 2e, multiplied by an arbitrary factor to make direct comparison the spectra easier. Notably, the Fe absorbance spectrum at low ω linearly increases with ω, as expected when the wavelength of the incident light shifts away from the diffraction limit. Besides this increase, there is no significant feature in the $(\alpha t)^2$ spectra of Fe sample, as would be expected for a metallic, and opaque, material. Accordingly, we consider the $LaMnPO_{1-x}F_x$ sample to be opaque, and E_{Gap}=0, when its lineshape resembles that of the Fe flake, and the spectral features are suppressed. Using this criterion, we conclude that the pressure at which undoped LaMnPO becomes opaque ($P^o_{x=0.00}$) is above 21.7 GPa, where the spectral feature is still visible, but below 24.7 GPa. Likewise, the pressure

of opacity for $LaMnPO_{0.96}F_{0.04}$ ($P^o_{x=0.04}$) lies between 19.5 GPa and 21.1 GPa. The decrease in P^o with doping suggests that higher dopings could reduce P^o further, and more highly doped $LaMnPO_{1-x}F_x$ samples could be metallized with relatively small pressures.

Complementary high pressure resistance (R) measurements of LaMnPO were carried out, and reported in[14]. They found that R of undoped LaMnPO is reduced with increasing pressure, until it saturates at pressures above 20 GPa, consistent with the pressure at which we identify E_{Gap}=0. The measured R values are plotted alongside our experimentally determined E_{Gap} in Fig. 2c. Generally, opacity at low energies arises from free carriers. Thus the observation of opacity, the saturation in resistance at pressures above 20 GPa, and the systematic reduction in E_{Gap} at lower pressures all suggest a metallic state has been induced via collapse of the band gap.

D. On the Nature of the High Pressure Metallic State

The calculated band structure is plotted in Fig. 3a,b, and c for pressures of 1 bar, 16 GPa, and 30 GPa. At 1 bar, the smallest direct energy gap is at the Γ point, and is 1.0 eV. At 16 GPa, the direct band gap at the Γ point is reduced in energy. However, LaMnPO also undergoes a tetragonal to orthorhombic structural transition which allows interband transitions at the M point, which are smaller in energy than those at the Γ point. These newly allowed interband transitions at the M point produce the intra-gap features observed in the absorption spectra, and highlighted in Fig. 2d and 2e. Increasing the pressure to 30GPa results in a fully closed gap, with many bands cross the Fermi energy, yielding a metallic system.

Further insight into the correlations in this system can be revealed by examining the partial density of states (PDOS) calculated when correlations are both neglected, and when they are included. Thus, in Fig. 4a, 4b, and 4c, we show the PDOS calculated using DFT. At 1 bar (Fig. 4a), the system is strongly metallic, with all orbitals possessing a non-zero PDOS at E_F (Energy=0). Increasing the pressure to 16.2 GPa (Fig. 4b) reduces the PDOS of most orbitals in the vicinity of E_F, with the exception of the xz and yz orbitals, which develop a sharp peak just below E_F. By 30 GPa (Fig. 4c), the PDOS is suppressed for all orbitals, most notably the x^2-y^2 and xy orbitals, which in fact become gapped. The PDOS calculated via DFT+DMFT reveals a significantly different trend. At 1 bar (Fig. 4d), DFT+DMFT predicts the PDOS of all orbitals is zero at E_F yielding an insulating system, as verified by experiments in the main text, and in Refs.[4,6]. The calculation at 16.2 GPa (Fig. 4e) indicates that most of the orbitals in LaMnPO develop a significant peak in the PDOS immediately below, and at approximately 0.1 eV above E_F. However, the electron correlations, though reduced by pressure, are still strong enough to sustain the energy gap. Finally, at 30 GPa (Fig. 4f), DFT+DMFT finds that the system is highly metallic, where all but the xy orbital has a non-zero PDOS at E_F.

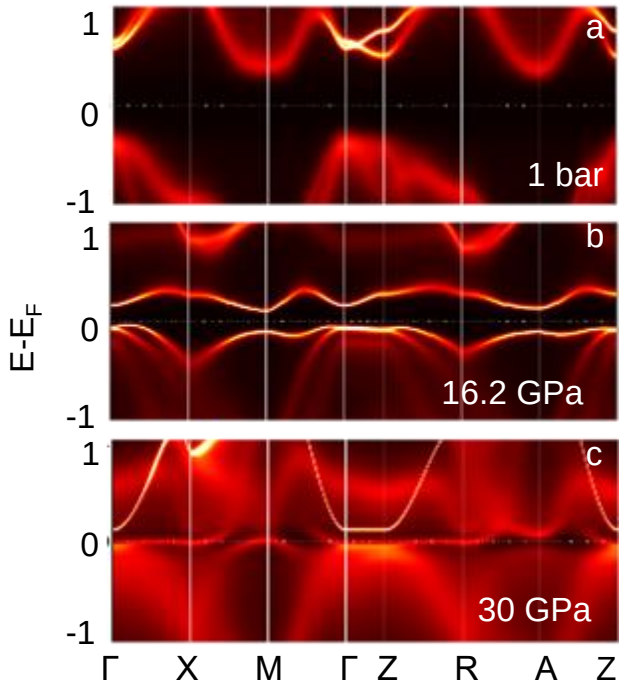

FIG. 3. The band structure of LaMnPO at 1 bar (a), 16.2 GPa (b) and 30 GPa (c), calculated using DFT+DMFT

It is particularly interesting to compare the PDOS obtained from DFT at 30 GPa, to the complementary DFT+DMFT PDOS at the same pressure. At this pressure, these two methods of calculation seem to produce qualitatively similar PDOS spectra for all orbitals. Typically, when DFT produces similar results to calculations where correlations are included, it indicates that the effect of the correlations on the electronic system have been largely reduced. However, the electronic bandwidth, corresponding to the width of the peak in PDOS near Energy = 0.0 eV, is still smaller in the DFT+DMFT calculations than those obtained from DFT, indicating correlations are still present. In the case of LaMnPO, this would mean that increasing the pressure from 16.2 GPa, to 30 GPa, tunes the system from a Mott-Hund's insulator to a correlated metal. The intermediate region between these two pressures warrants further study, as moderate correlations often herald a complex and exciting phase diagram, the most salient examples of this being the cuprates and Fe-pnictides[21–23]. However, this region remains largely unexplored, and the transmission is effectively zero in the metallic state, thus no useful data on the free carrier dynamics can be obtained using the spectroscopic transmission techniques utilized in this work. Future studies, both theoretical and experimental, are required to ascertain the landscape of this moderately correlated region of the phase diagram. One very likely outcome would be the revelation of an orbitally

selective Mott transition, which can be expected when Mott-Hubbard interaction and Hund's coupling are both present, and substantial crystal field splitting differentiates the Mn 3d orbitals, as in this class of material[21,24–26].

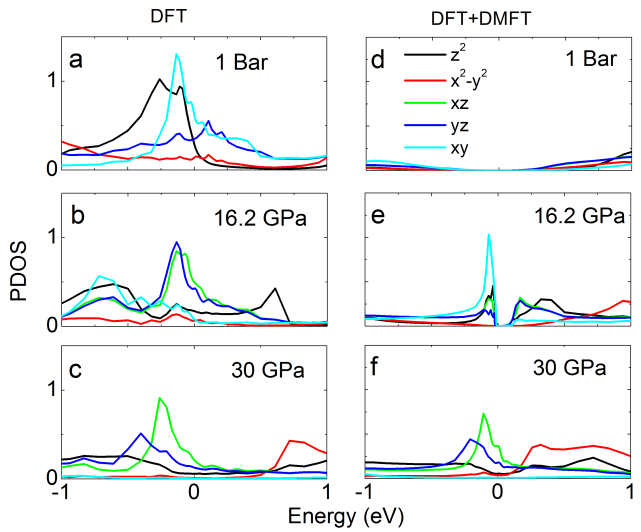

FIG. 4. The PDOS in LaMnPO is calculated using DFT at 1 bar (a) 16.2 GPa (b) and 30 GPa (c). Likewise, the PDOS extracted from DFT+DMFT at 1 bar (d), 16 GPa (e) and 30 GPa (f) is also shown

III. CONCLUSION

Our data reveal that by applying pressure to LaMnPO, we are able to induce a bulk metallic state, which is not directly caused by the elimination of AF order, or the structural transition. Furthermore, our results can be consistently described using DFT+DMFT, assuming the presence of AF ordering, a Mott-Hubbard U and Hund's rule J_H. The coexistence of these correlations suggest this system resembles the Fe-pnictides, albeit with an insulating ground state. These results also imply that the insulator-metal phase transition is shifted to lower pressures with F-doping. Our findings identify $LaMnPO_{1-x}F_x$ as an exciting playground in which the parameters of pressure and doping may be tuned to reveal a complex phase diagram, as is often found in strongly correlated systems.

IV. APPENDIX A: THEORETICAL CALCULATIONS

Density functional theory (DFT) band structure calculations were done using the full-potential linear augmented plane wave method implemented in Wien2K[27] in conjunction with a generalized gradient approximation[28] of the exchange correlation functional. To take into account strong correlation effect, we further carried out first-principles calculations using DFT+DMFT[29] which was implemented on top of Wien2k and documented in Ref.[30]. In the DFT+DMFT calculations, the electronic charge was computed self-consistently on DFT+DMFT density matrix. The quantum impurity problem was solved by the continuous time quantum Monte Carlo method[31,32], using Slater form of the Coulomb repulsion in its fully rotational invariant form. We used a Hubbard U=8.0 eV and Hund's rule coupling J=0.9 eV for all the DFT+DMFT calculations at all pressures, consistent with previous publication[12]. The Hamiltonian used for these calculations is:

$$\hat{H} = \sum_i (-\mu \hat{N}_i + \hat{H}_{int}[\hat{d}^\dagger_{i\nu}]) + \sum_{\langle ij\rangle\nu} t \hat{d}^\dagger_{i\nu} \hat{d}_{j\nu},$$

$$\hat{H}_{int}[\hat{d}^\dagger_{i\nu}] = \frac{3}{4} J \hat{N}_i + \frac{1}{2}\left(U - \frac{1}{2}J\right)\hat{N}_i(\hat{N}_i - 1) - J\hat{\mathbf{S}}_i^2.$$

In this Hamiltonian, $d^\dagger_{i\nu}$ is the creation operator on site i for an electron of type ν, where $\nu = (m\sigma)$, with σ and m indicating the electron spin and orbital, respectively[33]. Further details on the Hamiltonian and the theoretical methods can be found in[33]

We used the experimentally determined lattice structures[5], including the internal positions of the atoms as shown in Table I

V. APPENDIX B: ALTERNATIVE DETERMINATION OF E_{Gap}

If one has access to the complex dielectric constant ($\hat{\epsilon} = \epsilon_1 + i\epsilon_2$), the magnitude of E_{Gap} can be precisely determined from the x-axis intercept of a linear fit to $(\epsilon_2)^2$[17]. Accordingly, we measured the transmittance spectra over a broad range (100 cm^{-1} to 12,000 cm^{-1}) during some of the high temperature measurements, and modelled these spectra to obtain $\hat{\epsilon}$. Moreover, by simultaneously fitting the periodicity of the interference fringes, along with the transmittance amplitude, we accurately determined the thickness of these crystals to be 5 $(\pm 0.3)\mu m$. An example transmittance spectra, obtained at 295K, is shown in the inset to Fig. 5a (black line), along with the corresponding model (gray line). The resulting $(\epsilon_2)^2$ spectra, which were obtained at temperatures from 295K to 450K, are plotted in Fig. S2a (colored lines), along with the linear extrapolation at each temperature (gray lines). The values of E_{Gap} corresponding to this alternative analysis are plotted in Fig. 5b (filled black squares), along with the values of E_{Gap} obtained from the $(\alpha t/\omega)^2$ analysis (open black squares), described in the main text[17]. An inspection of Fig. 5a, reveals that the $(\alpha t/\omega)^2$ analysis tends to underestimate the value of E_{Gap} by approximately 300 cm^{-1}, and thus establishes the size of the error bars. Importantly, this difference is small when compared to the magnitude of the E_{Gap}. In addition, the $(\alpha t/\omega)^2$ analysis captures the overall behavior of E_{Gap}. Both of these latter facts confirm the validity

P (GPa)	Space group	a (Å)	b (Å)	c (Å)	z_{La}	z_P
0	P4/nmm (#129)	4.05786	4.05786	8.84341	0.13879	0.6569
3	P4/nmm (#129)	4.0350	4.0350	8.712	0.1415	0.6526
6	P4/nmm (#129)	4.0122	4.0122	8.581	0.1443	0.6512
9	P4/nmm (#129)	3.9945	3.9945	8.451	0.1425	0.6428
12	P4/nmm (#129)	3.9768	3.9768	8.322	0.1407	0.6345
14	P4/nmm (#129)	3.95344	3.95344	8.34822	0.1416	0.6260
16	Cmma (#67)	5.5937	5.6664	8.169	0.1485	0.612
30	Cmma (#67)	5.20408	5.37473	7.42454	0.1091	0.5676

TABLE I. Crystal parameters used in the electronic structure calculations

of this method for extracting E_{Gap}, and analyzing trends, particularly when one lacks the full ϵ_2 spectra.

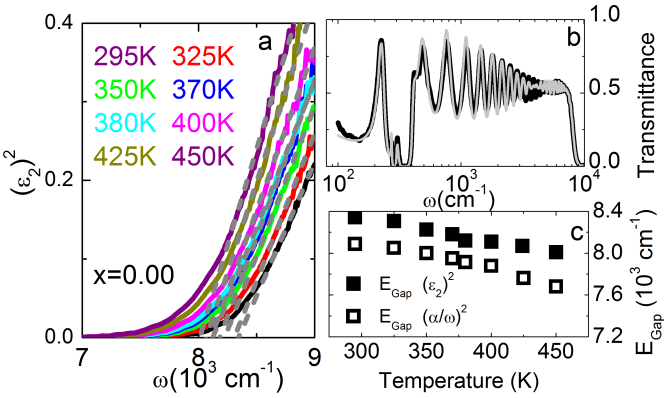

FIG. 5. (a) The $(\epsilon_2)^2$ spectra, obtained for undoped LaMnPO at a series of temperatures. The linear fits, which were used to determine E_{Gap} are indicated by the gray lines. (b) An example broadband transmittance spectra at 295K (black line), and the corresponding model fit (gray line) are shown. (c) The energy gap extracted using the linear fit to $(\epsilon_2)^2$ is plotted vs temperature (filled black squares), along with E_{Gap} obtained from the $(\alpha t/\omega)^2$ analysis (open black squares).

VI. ACKNOWLEDGEMENTS

We acknowledge the Office of the Assistant Secretary of Defense for Research and Engineering for providing the NSSEFF funds that supported this research (KWP, ZPY, JWS, SZ, DEM). Work at UCSD is supported by ARO w911NF-13-1-0210

[1] A. Pandey, V. K. Anand, and D. C. Johnston, Physical Review B **84**, 014405 (2011).

[2] A. Pandey, B. G. Ueland, S. Yeninas, A. Kreyssig, A. Sapkota, Y. Zhao, J. S. Helton, J. W. Lynn, R. J. McQueeney, Y. Furukawa, A. I. Goldman, and D. C. Johnston, Physical Review Letters **111**, 047001 (2013).

[3] A. T. Satya, A. Mani, A. Arulraj, N. V. C. Shekar, K. Vinod, C. S. Sundar, and A. Bharathi, Physical Review B **84**, 180515 (2011).

[4] J. W. Simonson, G. J. Smith, K. Post, M. Pezzoli, J. J. Kistner-Morris, D. E. McNally, J. E. Hassinger, C. S. Nelson, G. Kotliar, D. N. Basov, and M. C. Aronson, Physical Review B **86**, 184430 (2012).

[5] J. W. Simonson, Z. P. Yin, M. Pezzoli, J. Guo, J. Liu, K. Post, a. Efimenko, N. Hollmann, Z. Hu, H.-J. Lin, C.-T. Chen, C. Marques, V. Leyva, G. Smith, J. W. Lynn, L. L. Sun, G. Kotliar, D. N. Basov, L. H. Tjeng, and M. C. Aronson, Proceedings of the National Academy of Sciences of the United States of America **109**, E1815 (2012).

[6] J. W. Simonson, K. Post, C. Marques, G. Smith, O. Khatib, D. N. Basov, and M. C. Aronson, Physical Review B **84**, 165129 (2011).

[7] Y.-L. Sun, J.-K. Bao, Y.-K. Luo, C.-M. Feng, Z.-A. Xu, and G.-H. Cao, EPL (Europhysics Letters) **98**, 17009 (2012).

[8] T. Jungwirth, V. Novák, X. Martí, M. Cukr, F. Máca, A. B. Shick, J. Mašek, P. Horodyská, P. Němec, V. Holý, J. Zemek, P. Kužel, I. Němec, B. L. Gallagher, R. P. Campion, C. T. Foxon, and J. Wunderlich, Physical Review B **83**, 035321 (2011).

[9] D. C. Johnston, R. J. McQueeney, B. Lake, A. Honecker, M. E. Zhitomirsky, R. Nath, Y. Furukawa, V. P. Antropov, and Y. Singh, Physical Review B **84**, 094445 (2011).

[10] J. G. Cheng, K. Matsubayashi, W. Wu, J. P. Sun, F. K. Lin, J. L. Luo, and Y. Uwatoko, Physical Review Letters **114**, 117001 (2015).

[11] A. Georges, L. de' Medici, and J. Mravlje, Annual Review of Condensed Matter Physics **4**, 137 (2013), http://dx.doi.org/10.1146/annurev-conmatphys-020911-125045.

[12] D. E. McNally, J. W. Simonson, K. W. Post, Z. P. Yin, M. Pezzoli, G. J. Smith, V. Leyva, C. Marques, L. DeBeer-Schmitt, A. I. Kolesnikov, Y. Zhao, J. W. Lynn, D. N. Basov, G. Kotliar, and M. C. Aronson, Physical Review B **90**, 180403 (2014).

[13] D. Basov and T. Timusk, Reviews of modern physics **77**, 721 (2005).

[14] J. Guo, J. W. Simonson, L. Sun, Q. Wu, P. Gao, C. Zhang, D. Gu, G. Kotliar, M. Aronson, and Z. Zhao, Scientific reports **3**, 2555 (2013).

[15] C. C. Katsidis and D. I. Siapkas, Appl. Opt. **41**, 3978 (2002).

[16] M. Dressel and G. Gruener, *Electrodynamics of Solids: Optical Properties of Electrons in Matter*, 1st ed., Vol. 70

(Cambridge University Press, New York, New York, USA, 2002).
[17] M. Yu, Peter Y., Cardona, *Fundamentals of Semiconductors. Graduate Texts ...* (2010).
[18] A. Comanac, L. de' Medici, M. Capone, and A. J. Millis, Nature Physics **4**, 287 (2008).
[19] G. Kotliar and D. Vollhardt, Physics Today **57**, 53 (2004).
[20] A. Goncharov, V. Struzhkin, R. Hemley, H. Mao, and Z. Liu, Science and technology of high pressure , 90 (2000).
[21] L. de'Medici, G. Giovannetti, and M. Capone, Physical Review Letters **112**, 177001 (2014), 1212.3966.
[22] M. Qazilbash, J. Hamlin, and R. Baumbach, Nature Physics **5**, 5 (2009).
[23] D. N. Basov and A. V. Chubukov, Nature Physics **7**, 272 (2011).
[24] L. de'Medici, Physical Review B **83**, 205112 (2011).
[25] L. de' Medici, S. R. Hassan, M. Capone, and X. Dai, Physical Review Letters **102**, 126401 (2009).
[26] Z. P. Yin, K. Haule, and G. Kotliar, Nature materials **10**, 932 (2011).
[27] P. Blaha, K. Schwarz, G. K. H. Madsen, D. Kvasnicka, and J. Luitz, *WIEN2K, An Augmented Plane Wave + Local Orbitals Program for Calculating Crystal Properties* (Karlheinz Schwarz, Techn. Universität Wien, Austria, 2001).
[28] J. P. Perdew, K. Burke, and M. Ernzerhof, Phys. Rev. Lett. **77**, 3865 (1996).
[29] G. Kotliar, S. Y. Savrasov, K. Haule, V. S. Oudovenko, O. Parcollet, and C. A. Marianetti, Rev. Mod. Phys. **78**, 865 (2006).
[30] K. Haule, C.-H. Yee, and K. Kim, Phys. Rev. B **81**, 195107 (2010).
[31] K. Haule, Phys. Rev. B **75**, 155113 (2007).
[32] P. Werner, A. Comanac, L. de' Medici, M. Troyer, and A. J. Millis, Phys. Rev. Lett. **97**, 076405 (2006).
[33] K. M. Stadler, Z. P. Yin, J. von Delft, G. Kotliar, and A. Weichselbaum, Phys. Rev. Lett. **115**, 136401 (2015).